ADVANCED FUNCTIONAL MATERIALS
www.afm-journal.de

Chemically Tailored Metal-Organic Frameworks for Enhanced Capture of Short- and Long-Chain Per- and Polyfluoroalkyl Substances from Water

Edward Loukopoulos, Sergio Marugán-Benito, Dionysios Raptis, Emmanuel Tylianakis, George E. Froudakis, Andreas Mavrandonakis,* and Ana E. Platero-Prats**

Per- and polyfluoroalkyl substances (PFAS) are emerging as bioaccumulative and toxic water pollutants, posing a large threat to human and aquatic organisms. This threat is aggravated by their extreme persistence to common degradation methods. Adsorption is regarded as the most conventional method to treat these contaminants, however, existing sorbents present considerable limitations on performance. The development of more efficient PFAS adsorbents is therefore of urgent need. The class of metal-organic frameworks (MOFs) can hold great promise for these purposes, featuring porous materials with high tailoring potential. Herein, a series of functionalized Zr-MOFs have been designed with boosted capacities for the adsorption of short- and long-chain perfluorinated carboxylic acids of environmental interest. The approach relies on chemistry-based concepts to introduce targeted post-synthetic modifications that promote PFAS···MOF interactions, specifically through coordinative bonding and hydrophobic effects. In particular, the framework TFA-MOF-808 (TFA = trifluoroacetic acid) displays the highest capture capacities reported for MOF materials in this pollutant class. Mechanistic studies, assisted by advanced synchrotron characterization techniques and theoretical calculations, support a ligand exchange process occurring during the adsorption phenomena. The results demonstrate the potential of this design approach in developing advanced PFAS sorbents with optimal performance.

1. Introduction

The emergence of persistent anthropogenic pollutants has significantly impeded ongoing global efforts to improve water quality. Per- and polyfluoroalkyl substances (PFAS) represent a key example of such contaminants[1] and have been the subject of several directives and regulations worldwide.[2] Chemicals of this family contain a fluorinated carbon chain backbone, typically terminated by a hydrophilic functional group.[3] They are widely used in industrial practices, as their strong C—F bonds bestow them with exceptional properties including high stability, hydro-/oleo-phobicity, and high surface activity.[4] At the same time, these characteristics make them extremely difficult to break down with conventional wastewater treatment methods,[5] leading to high bioaccumulation and adverse effects on human organisms and the environment.[6] As a result, PFAS-contaminated waters are most commonly treated using adsorption-based technologies, involving filtration through activated carbons or ion-exchange resins.[7] Both sorbents, however, display limitations such as lower adsorption capacities for short-chain analogs, as well as slow adsorption kinetics.[7,8] Hence, it is imperative to develop smart porous materials as advanced PFAS sorbents with a very high capacity and efficient removal capabilities, irrespective of chain length.

E. Loukopoulos, S. Marugán-Benito, A. E. Platero-Prats
Departamento de Química Inorgánica
Facultad de Ciencias
Universidad Autónoma de Madrid
Campus de Cantoblanco, Madrid 28049, Spain
E-mail: edouardos.loukopoulos@uam.es; ana.platero@uam.es

The ORCID identification number(s) for the author(s) of this article can be found under https://doi.org/10.1002/adfm.202409932

DOI: 10.1002/adfm.202409932

D. Raptis, G. E. Froudakis
Department of Chemistry
University of Crete
Heraklion 71003, Greece

E. Tylianakis
Department of Materials Science and Technology
University of Crete
Heraklion, Crete 71003, Greece

A. Mavrandonakis
Material Science Institute of Madrid (ICMM-CSIC)
Sor Juana Inés de la Cruz 3, Cantoblanco, Madrid 28049, Spain
E-mail: andreas.mavrantonakis@icmm.csic.es

A. E. Platero-Prats
Condensed Matter Physics Center (IFIMAC)
Universidad Autónoma de Madrid
Campus de Cantoblanco, Madrid 28049, Spain

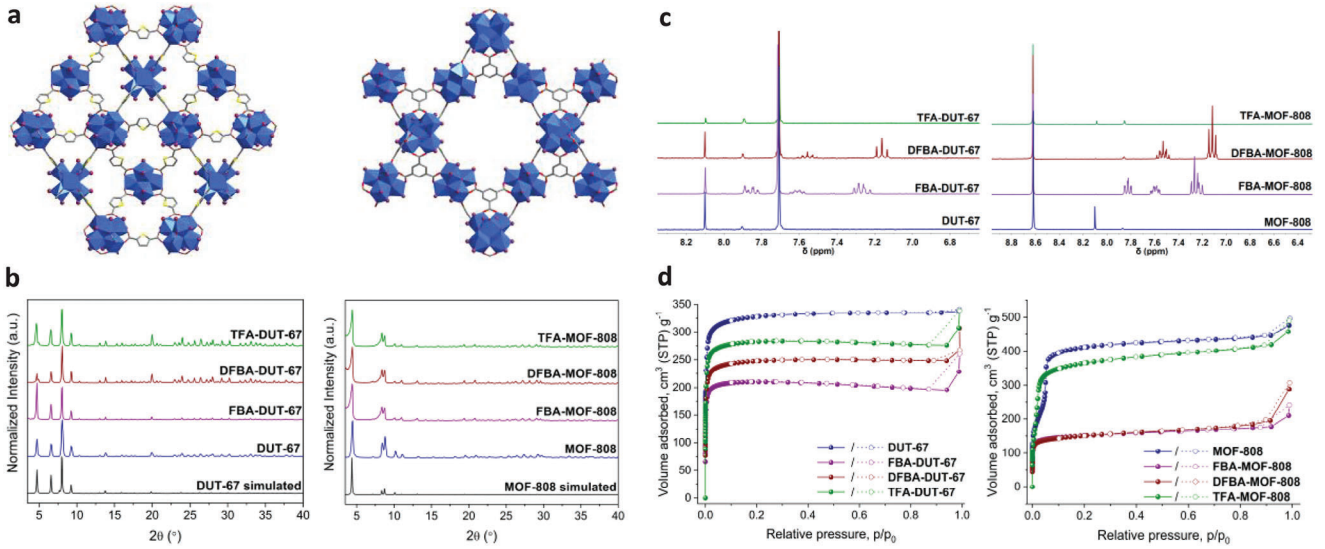

Figure 1. a) View of the main framework and pore systems in DUT-67 (left) and MOF-808 (right). Color coding: Zr polyhedral = blue, C = grey, O = red. Potentially available positions for ligand functionalization within the inorganic nodes are depicted as dark red spheres. H atoms have been omitted for clarity. b—d) PXRD data, ^{1}H NMR spectra, and N_2 isotherms (recorded at 77 K) of the pristine and functionalized DUT-67 and MOF-808 materials.

On this basis, metal-organic frameworks (MOFs) have also begun to gain traction as potential platforms for PFAS removal. As a unique class of porous hybrid inorganic-organic materials, MOFs offer an immense amount of control and tuning through the limitless combinations of organic linkers and inorganic building units.[9] This can enable the synthesis of tailor-made MOFs with unique targeted characteristics (e.g., exceptionally high porosity, rapid adsorption kinetics, water and thermal stability, regeneration and reuse capabilities) that render them as ideal materials for various environmental applications.[10] However, despite the growing number of studies, research on PFAS remediation remains in its early stages. Existing reports focus on pristine MOF materials and their application in the removal of mostly particular long-chain PFAS such as perfluorooctanoic acid (PFOA) or perfluorooctanesulfonic acid.[8b,11] To fully harness the capabilities of MOFs as PFAS sorbents, conducting more systematic studies is crucial, leveraging the available tuning options for structural composition and pore environment of the materials. In this work, we exploit the effect of PFAS···MOF interactions to design tailor-made porous frameworks with significantly enhanced adsorption capacities for both short- and long-chain perfluoroalkyl carboxylic acids. To achieve this goal, we have synthesized two different families of Zr-based MOFs through post-synthetic incorporation of carefully selected organic ligands.

2. Synthesis and Characterization of Pristine and Functionalized MOFs

To initiate our investigations, prototypical MOFs DUT-67[12] and MOF-808[13] were selected and synthesized. These frameworks were chosen based on several criteria: exceptional water stability, high purity and yield achievable through green synthetic procedures.[14] Additionally, they exhibit suitable porosity to accommodate PFAS of varying chain lengths and kinetic diameters (DUT-67 features inner cuboctahedral and octahedral cages of 14.2 and 11.7 Å diameter, while MOF-808 contains hexagonal channels of ≈18 Å). Importantly, both frameworks have unsaturated inorganic nodes based on Zr_6 clusters (8-connected in DUT-67, 6-connected in MOF-808), providing an excellent platform for chemical tailoring to modify and enhance their properties (**Figure 1a**).[15] Successful synthesis of both materials in highly crystalline form was confirmed through detailed characterization by Powder X-ray Diffraction (PXRD), ^{1}H Nuclear Magnetic Resonance (NMR), Fourier-transform Infrared Spectroscopy (FT-IR), Thermogravimetric Analysis (TGA), Scanning Electron Microscopy (SEM) and gas adsorption (Figure 1b–d and Sections S1–S7, Supporting Information).

The pristine MOFs were then functionalized by incorporating a fluorine-containing monocarboxylic acid as a non-structural ligand within the Zr_6 clusters, in particular 2-fluorobenzoic acid (FBA), 2,6-difluorobenzoic acid (DFBA) or trifluoroacetic acid (TFA). This strategy enabled precise control of the size and hydrophobicity of the MOF pores by adjusting the amount of fluorine or introducing bulkier benzoate groups. The corresponding FBA-/DFBA-/TFA-MOFs were successfully obtained through post-synthetic modifications by immersing the pristine MOF in a solution of the respective monocarboxylic ligand (See Section S1, Supporting Information). PXRD studies showed that the main frameworks and crystallinity are retained in all cases (Figure 1c; Section S2, Supporting Information). The morphology of the crystals and particle size also remained unaltered, as demonstrated by SEM images (Figures S33–S38, Supporting Information). Evidence of the presence of the monocarboxylate ligands within the corresponding MOFs was gained through a combination of ^{1}H- and ^{19}F-NMR experiments. In agreement with reported data[16] on the functionalization of DUT-67, a partial insertion of fluorinated ligand was consistently achieved when employing larger ligands (2 FBA, 1 DFBA, and 3.9 TFA molecules per Zr_6 cluster). On the other hand, a higher degree of

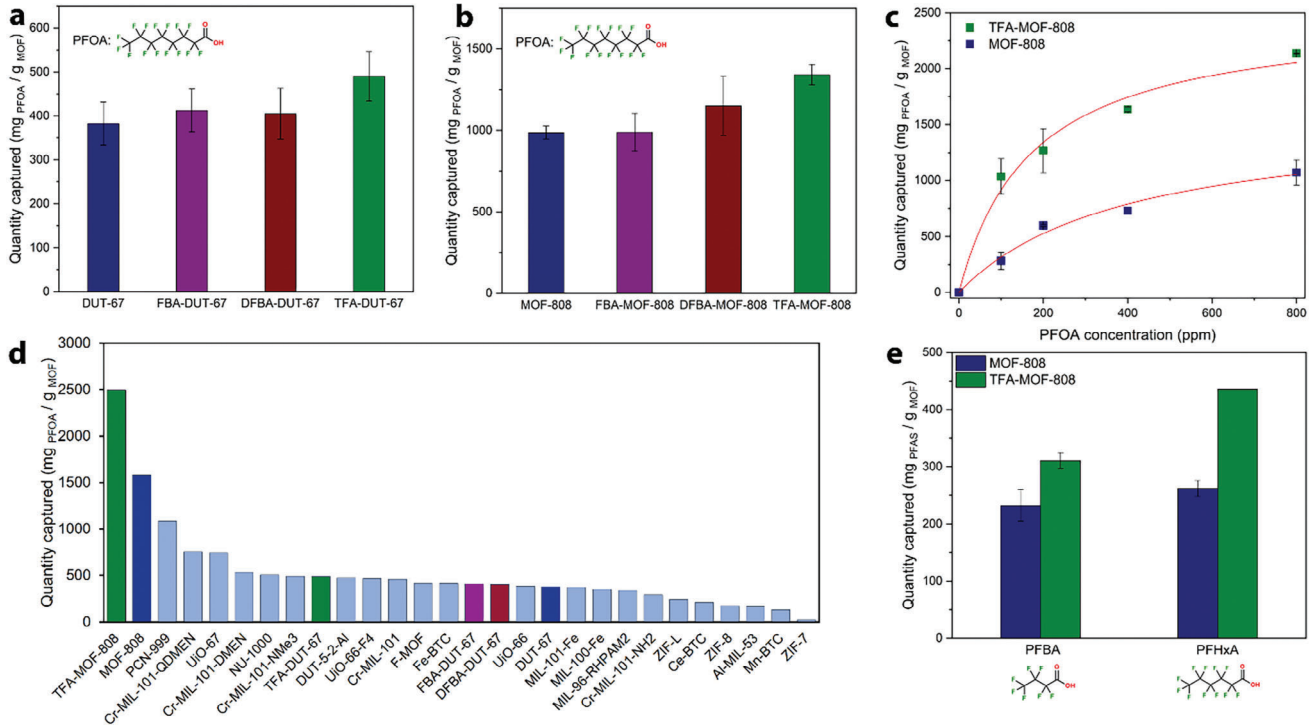

Figure 2. a) PFOA adsorption capacity screenings for the DUT-67 analogs. Experimental conditions: $[PFOA]_0$ = 500 ppm, [MOF] = 10 mg/10 mL of PFAS solution. b) PFOA adsorption capacity screenings for the MOF-808 analogs. Experimental conditions: $[PFOA]_0$ = 800 ppm, [MOF] = 3 mg/20 mL of PFAS solution. c) PFOA adsorption isotherms of TFA-MOF-808 and pristine MOF-808. [MOF] = 3 mg/20 mL of PFAS solution. Squares = adsorption data, solid lines = Langmuir fits. d) PFOA adsorption performance of all reported MOF materials, including the ones presented in this work. Detailed data and relevant references are found in Table S7 (Supporting Information). e) PFBA and PFHxA adsorption capacity screenings for pristine MOF-808 and TFA-MOF-808. Experimental conditions: $[PFAS]_0$ = 100 ppm, [MOF] = 3 mg/20 mL of PFAS solution. All experiments were performed at least two times and average values are reported.

post-synthetic incorporation was accomplished in the MOF-808 analogs. NMR analysis revealed the presence of 4.5 FBA, 5 DFBA, and 4.2 TFA molecules per Zr_6 node, along with the complete removal of formate ligands from the cluster (see Sections S1 and S3, Supporting Information).[17] As detailed in Section S5 (Supporting Information), the FT-IR spectra of the functionalized materials also revealed additional signals compared to the pristine MOFs. These were found to be consistent with the appearance of an extra benzene ring (880 cm^{-1}, only observed for the FBA-/DFBA- analogs) and the presence of C—F bonding (1090, 1160, 1205, and 1225 cm^{-1}, depending on the fluorinated ligand). N_2 sorption studies on the functionalized MOFs showed notably reduced uptake and specific surface areas compared to the pristine materials (Figure 1d; Section S6, Supporting Information). Similar variations were observed in the corresponding pore size distribution and pore volume contributions. These results align well with the incorporation of secondary ligands of various sizes within the inorganic clusters, located pointing toward the larger pore apertures.

3. PFAS Capture Experiments

3.1. Long-Chain PFAS

Having established the identity of all materials, initial screenings for PFAS capture were performed by exposing predetermined amounts of MOF to aqueous PFOA solutions (500/800 ppm) for 24 h (See Section S8, Supporting Information for more details). The amount of adsorbed pollutant was calculated as the difference between starting and ending PFAS concentration within the solution, as determined through ^{19}F-NMR spectroscopy.[18] The capture capacity performance (mg_{PFAS}/g_{MOF} adsorbed) was then quantified accordingly. From these screenings, pristine DUT-67 was found to adsorb 383 mg_{PFOA}/g_{MOF}, displaying moderate capture capability compared to the respective values for other MOF materials in the literature (**Figure 2**; Table S4, Supporting Information). On the other hand, pristine MOF-808 exhibited a remarkable ability to adsorb PFOA using very low MOF dosages (0.15 mg_{MOF} mL^{-1}), indicating excellent capture capacity. When immersed to an 800 ppm aqueous solution of the contaminant, the material demonstrated a PFOA uptake of 986 mg g^{-1}, surpassing all previously reported frameworks under these conditions. Importantly, the use of the FBA-/DFBA-/TFA-decorated materials resulted in a notable increase in uptake quantity for both Zr-MOF families, up to 28% (490 mg g^{-1}) in TFA-DUT-67 and 36% (1341 mg g^{-1}) in TFA-MOF-808 (Figure 2a,b; Table S5, Supporting Information). This performance was also observed in MOF batches of various particle sizes (crystallites of ≈100–200 or ≈200–400 nm). Driven by the results of the MOF-808 series, we then conducted PFOA adsorption isotherm studies for the pristine framework and the highest performing TFA-functionalized material, covering pollutant concentrations

ranging from 100 to 800 ppm. As shown in Figure 2c and Table S6 (Supporting Information), the functionalized MOF significantly outperforms the pristine analog across this concentration range and under the same experimental conditions. It is worth noting that the capture data were well fitted using either the Langmuir or Freundlich adsorption models, resulting in high correlation coefficients in both cases (Figures S67–S70, Supporting Information). This behavior provides valuable insights into the mechanism of pollutant capture, which will be discussed in detail in Section 4, along with other findings. Slightly better fits were obtained using the Langmuir model, allowing us to calculate the maximum PFOA adsorption capacity of MOF-808 and TFA-MOF-808, found to be 1581 and 2496 mg g^{-1} respectively. These results underscore the excellent capture capabilities of these materials, with their capacity values being multiple times larger than the highest-performing MOFs reported in the literature (Figure 2d; Table S7, Supporting Information). In terms of pollutant removal performance, TFA-MOF-808 achieved a 100% removal efficiency at low (100 ppm) contaminant levels despite the low MOF dosing, indicating high potential at environmentally relevant concentrations.[19] In comparison, only 30% of PFOA is removed when pristine MOF-808 is employed under the same conditions (Figure S71, Supporting Information).

3.2. Short-Chain PFAS

The use of long-chain PFAS (C ≥ 8 for carboxylic acid analogs) has faced gradual restrictions since the mid-2000s, ultimately leading to the EU ban on PFOA in 2020.[2b] Consequently, they have been replaced in the industrial sector by shorter-chain PFAS, eventually leading to their own increased bioaccumulation and toxicity.[20] At the same time, these pollutants also exist in the environment as the degradation products from several PFA precursors (e.g., alcohols, esters, and longer carboxylic acids).[20c,21] Given these concerns, along with the aforementioned limitations of current adsorption technologies, it becomes essential to develop materials capable of adsorbing these pollutants from water sources. As a proof of concept, representative materials MOF-808 and TFA-MOF-808 were tested for the adsorption of perfluorohexanoic (PFHxA, C = 6) and perfluorobutanoic (PFBA, C = 4) acid. Compared to PFOA, capture of these molecules is typically less reliant on hydrophobic interactions due to their shorter chain length and the presence of fewer fluorine atoms. Therefore, the post-synthetic incorporation of additional hydrophobicity into the MOF is even more crucial in order to enhance PFAS affinity in such cases. As shown in Figure 2e and in the Supporting Information (Figure S71, Table S8, Supporting Information), when immersed in an aqueous solution containing 100 ppm of pollutant, TFA-MOF-808 offers significant boosts in uptake quantity (66% for PFHxA, 33% for PFBA) and removal efficiency (40% for PFHxA, 12% for PFBA) compared to the non-fluorinated material. Remarkably, the respective calculated capacities (436 mg_{PFHxA} g^{-1} and 311 mg_{PFBA} g^{-1}) place TFA-MOF-808 among the top-performing porous materials for the capture of both pollutants in such concentrations. To the best of our knowledge, these values well exceed the reported uptakes for other materials including MOFs, covalent-organic frameworks, activated carbon-based substances, hydrogels, and zeolites (Table S9, Supporting Information). The results demonstrate that the functionalization approach can be key in the development of universal sorbents for perfluoroalkyl carboxylic acids, leading to enhanced performances regardless of chain length.

4. Mechanistic Investigations

4.1. Post-Capture Characterization

Motivated by the capture results, we embarked on gaining further insight on the mechanistic intricacies of these phenomena by characterizing the solid materials obtained post-PFAS capture. PXRD and SEM analysis, detailed in Sections S2 and S4 (Supporting Information), showed that the frameworks retain crystallinity and structural integrity in all cases, while the size and shape of the particles also remain unchanged compared to the pre-capture solids. FT-IR measurements revealed the appearance of additional bands at the 1400–1000 cm^{-1} region, in line with the presence of new C—F bonds determined by the nature of the fluorinated contaminant (Figures S47 and S48, Supporting Information). TGA analysis for all materials (Section S7, Supporting Information) showed increased mass loss, in agreement with the decomposition of added PFOA molecules. This process begins at the range of 315 °C, long after the boiling point of PFOA (189 °C), indicating strong interactions between the MOF and the contaminant.

Crucially, a series of ^{1}H- and ^{19}F-NMR studies revealed the incorporation of PFAS contaminant molecules per Zr_6 node, also accompanied by a loss of the initial non-structural ligand (Figures S26–S32, Supporting Information). This behavior was also observed in the functionalized materials during ^{19}F-NMR analysis of the post-capture solution, with additional peaks at either –114.9, –117.2, or –77.6 ppm due to the respective presence of FBA, DFBA, or TFA (Figure S72, Supporting Information). These results suggest that an exchange of non-structural organic ligands occurs during the contaminant capture (**Figure 3a**), attributed to the strong acidity of PFOA compared to FBA, DFBA, and TFA (respective pKa values of –0.5, 3.27, 2.85, and 0.23).[8b] The effect of this exchange appears to be more ample in the more hydrophobic TFA-MOFs (Table S10, Supporting Information). Up to now, insertion of PFAS to unsaturated Zr_6 sites has also been observed for the materials NU-1000 and PCN-999, involving solely exchange with coordinated labile $^{-}$OH and H_2O groups.[22] Chemical analysis of TFA-MOF-808 solids after capture of PFOA in various concentrations (100–800 ppm) was also performed. As shown in Table S11 and Figure S73 (Supporting Information), the incorporation of pollutant molecules per Zr_6 cluster increases as the initial concentration increases, reaching a maximum of 3.6 PFOA, presumably due to pore size restrictions. This result demonstrates that a considerable amount of the capture is due to the coordinative bonding of the PFAS to unsaturated sites of the Zr_6 nodes. The remaining available sites are capped by terminally coordinating $^{-}$OH and H_2O groups, which have also been reported to participate in H-bonding interactions with the PFAS molecules, further favoring adsorption.[8b] In line with these observations, the presence of fewer unsaturated sites in the DUT-67 family (maximum of 4 per node) leads to inferior performance compared to the MOF-808 materials (maximum of 6 per node), despite the suitability of the former in pore size.

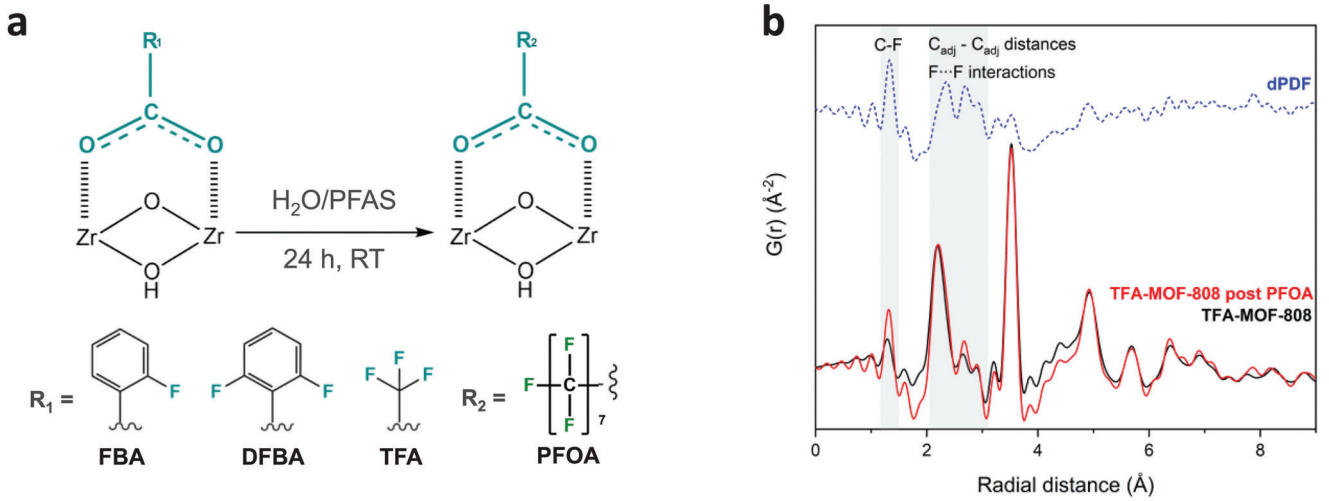

Figure 3. a) Schematic representation of the ligand exchange occurring during PFAS adsorption experiments. b) PDF data of TFA-MOF-808 before and after PFOA capture, including the corresponding dPDF signal.

As evidenced in Table S11 (Supporting Information), filling of the pore with additional PFAS molecules also occurs concurrently with these phenomena, further aided by the increased hydrophobicity of the inner surface when fluorinated ligands are also present. The existence of multiple driving forces of adsorption in the MOF-808-based materials is also supported by the excellent fits of the PFOA capture data using either of the Langmuir or Freundlich models, as mentioned earlier in the text. It should also be noted that, while the framework of MOF-808 is heteroporous, PFOA adsorption is only expected within the hexagonal mesopore. The possibility of another adsorption site within the small tetrahedral cage (diameter of ≈4.8 Å) can be excluded due to the large molecular length of the adsorbate.[23]

Pair distribution function (PDF) analysis of synchrotron X-ray total scattering data was also performed (Section S9, Supporting Information) in order to probe potential structural changes within the local environment of the materials after PFOA capture. PDF data collected in all materials of this study (pre- and post-PFOA) reveal three main signals centered at ca. 2.2, 3.5, and 5.0 Å (Figures S75–S78, Supporting Information). These signals are characteristic of the presence of Zr_6O_8 clusters, corresponding to Zr–O, Zr···Zr, and Zr···Zr_{axial} distances respectively.[24] To further assess the effect of the pollutant in the local structure, including the formation of PFAS···MOF interactions, differential analyses of the PDF data (dPDF) were also carried out for TFA-MOF-808 as the most optimal sorbent of this study. This was performed by comparing the respective PDFs before and after PFOA capture, subtracting one profile from the other to identify the associated contributions (Figure 3b). Further confirming the incorporation of PFOA within the Zr_6 nodes, the corresponding dPDF data reveal a sharp peak centered at ca. 1.3 Å, associated with the presence of C—F bonds.[25] Additional signals are also observed in the region of ca. 2.3–3.0 Å, specifically centered at 2.4, 2.7, and 2.9 Å. Matching the distances observed in crystal structures of perfluorinated carboxylic acids,[22b,25,26] the former signal can be assigned to the distance between adjacent carbon atoms of the perfluoroalkyl chain, while the remaining values are in excellent agreement with the formation of strong F···F interactions with varying C–F···F–C torsion angles.[27] Overall, these findings suggest a complex adsorption mechanism, based on hydrophobic interactions and coordinative bonding through ligand exchange. TFA-MOF-808 offers the optimal combination of node composition, pore size, and environment to promote these phenomena, leading to superior performance.

4.2. Theoretical Studies

To gain further insights into the adsorption of PFAS, Density Functional Theory (DFT) and Grand Canonical Monte Carlo (GCMC) calculations were performed. DFT calculations were employed in order to assess the thermodynamics for the binding of PFOA to the Zr_6-nodes, while GCMC was used to estimate the uptake of the MOFs. Due to the exceptional uptake of MOF-808 and its functionalized analogs, we decided to focus on the TFA-MOF-808 and pristine MOF-808 systems. Details about the DFT and GCMC calculations and the MOF models are given in the ESI (Section S10, Supporting Information). The free energies for the replacement of formate (or TFA) ligands in the pristine- (TFA-modified) MOF-808 respectively, with one and four PFOA molecules, have been computed. The results show that the binding of the first PFOA molecule is spontaneous to both pristine- and TFA-MOF-808, with their corresponding free energies computed to be −77.0 and −65.0 kJ mol^{-1}. The binding of four PFOA molecules to the TFA-MOF-808 is computed more exergonic with a reaction-free energy of −91.2 kJ mol^{-1}, while it becomes less favorable for the pristine MOF with a reaction-free energy of −7.3 kJ mol^{-1}. These DFT results are in line with the experimental observations, where four PFOA molecules can be added to the Zr_6 nodes of the TFA-MOF-808 via replacement of the TFA ligands, while this is not observed for the pristine MOF-808.

Furthermore, to rationalize the different capture capacities of MOF-808 and TFA-MOF-808 at low and high pollutant concentrations, GCMC simulations were utilized. Four different MOF-808 systems are studied: i) pristine (MOF-808), where four

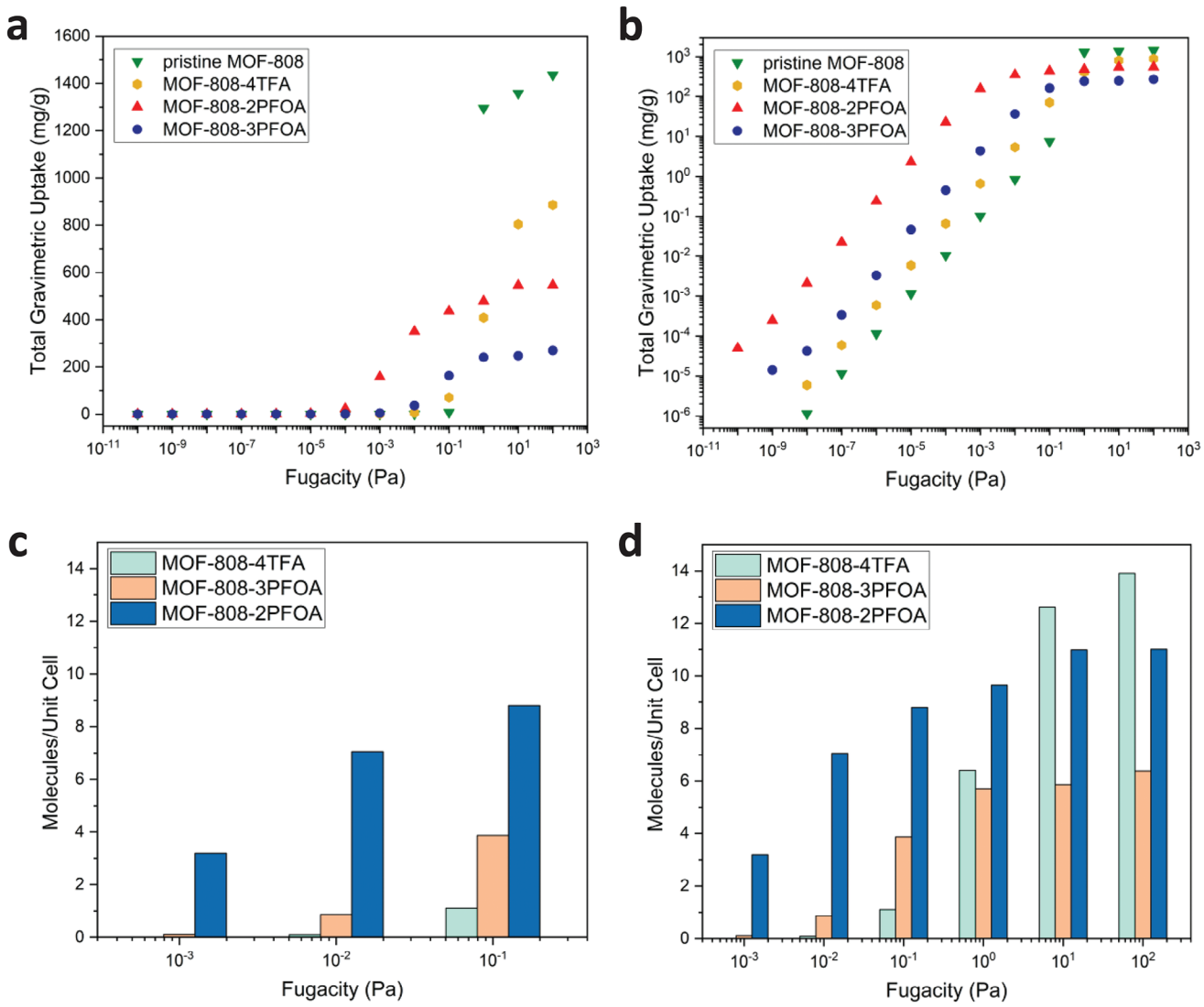

Figure 4. a,b) GCMC-simulated capture capacities (in semi-linear and logarithmic scales respectively) of the studied MOF-808 systems, highlighting the differences depending on the concentration of the pollutant. c,d) Uptake of PFOA molecules over different pollutant concentrations for the fluorinated MOF-808 systems.

formate ligands are present, and modified MOF-808 with ii) 2 PFOA (2PFOA-MOF-808), ii) 3 PFOA (3PFOA-MOF-808), and iv) 4 TFA (4TFA-MOF-808) ligands. The composition of the four systems is explained in detail in the ESI (Section S10, Supporting Information), and the GCMC results are presented in **Figure 4** and the ESI (Figure S83, Supporting Information). The uptake is plotted versus the fugacity, where fugacity is the effective partial pressure of the liquid PFOA in equilibrium with its vapor. Fugacity is analogous to the concentration. The results suggest that at high pollutant concentrations, MOF-808 has the highest uptake, followed by the 4TFA-MOF-808, while the PFOA-MOF-808 systems show the lowest capacity. This can be attributed to the more efficient packing of pollutant molecules because of the larger free space inside the pores. On the contrary, the 2PFOA- and 3PFOA-MOF-808 systems exhibit higher uptake at low pollutant concentrations than the MOF-808 or the TFA-MOF-808 systems.

This different capture behavior in low and high loadings can be attributed to the presence of the fluorinated ligands attached to the Zr_6 cluster that can create a hydrophobic environment in the pores. The 2PFOA- and 3PFOA-MOF-808 systems possess a higher hydrophobic character due to their larger fluorine content, thus more PFOA molecules can be inserted into the pores, compared to the less hydrophobic environment of the 4TFA-MOF-808. This is depicted in **Figure 5**, where a snapshot of the location of the physisorbed PFOA molecules inside the 4TFA-MOF-808 and 2- and 3-PFOA-MOF-808 is presented as computed from the GCMC simulations at low concentrations. Interestingly, PFOA molecules are found only in the small cages of the TFA-MOF-808, while only in the pores of the 2- and 3-PFOA-MOF-808. This different behavior can be attributed to the less hydrophobic environment of the pores of TFA-MOF-808.

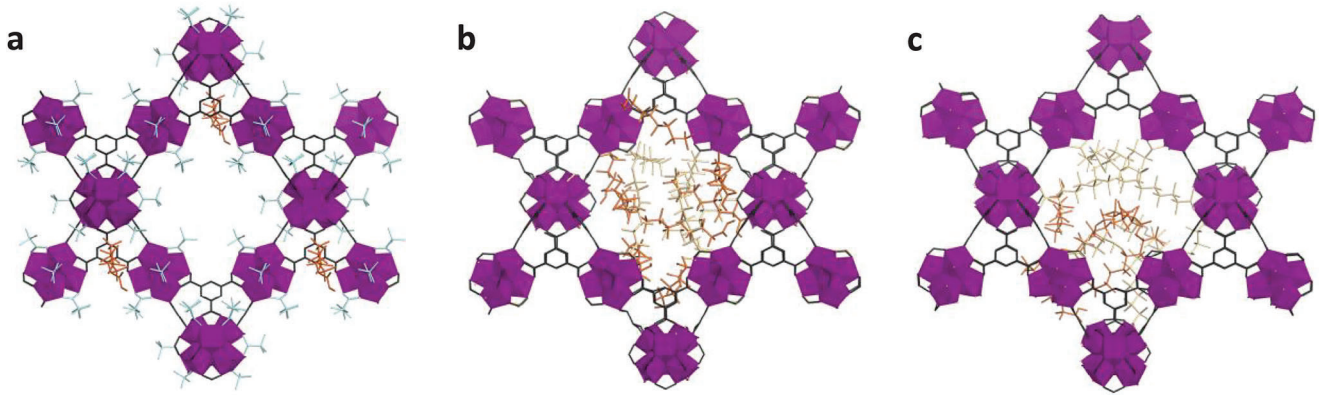

Figure 5. GCMC-simulated snapshots of a) 4TFA-MOF-808, b) 2PFOA-MOF-808, and c) 3PFOA-MOF-808 at 298K and 0.1 Pa. Color scheme: Zr – purple polyhedra, main organic linkers – black, TFA – turquoise. PFOA molecules physically adsorbed in the pores are shown in orange color, and PFOA molecules chemically adsorbed in the cluster nodes are shown in light yellow color.

5. Regeneration and Recyclability Tests

Having established the capture capabilities of TFA-MOF-808, we then attempted to determine its application potential for practical water decontamination in terms of regeneration and recyclability (Section S8, Supporting Information). Existing MOF regeneration studies typically involve the use of various solutions (acidic, basic, or organic) in order to remove the pollutant from the material.[8b] In our case, however, such treatments would lead to the pristine framework due to the associated ligand exchange taking place during the first adsorption cycle. To avoid this, direct regeneration of the material was achieved instead by employing the initial functionalization procedure described in Section 2. In this case, introduction of the PFOA-loaded MOF to a solution containing TFA excess is sufficient to favor reverse ligand exchange phenomena, enabling the formation of the TFA-decorated framework in a one-step process without any loss in crystallinity or stability (Figure S12, Supporting Information). As seen in Figure S74 (Supporting Information), the material can be then reused for at least 3 PFOA adsorption cycles, retaining complete (100%) removal efficiency. These results confirm the potential of these materials, while also validating the ability of the functionalization strategy. On the other hand, the practical application of TFA-MOF-808 for more industrial uses remains limited due to the associated ligand exchange mechanism (releasing environmentally harmful TFA during capture) and the suboptimal aspects of the current regeneration/recycling method (temperature requirements, loss of material during workups between cycles). We envision that the design of tailored MOFs with ideal real-life applications can be certainly achieved by researchers using the knowledge gained in this work, and efforts to develop such materials and protocols are currently underway in our group.a

6. Conclusion

In conclusion, we have utilized the tuning potential in MOFs with unsaturated metal sites to develop a new series of tailor-made materials for the adsorption of perfluorinated carboxylic acid pollutants from water. The introduction of targeted chemistry-based functionalizations has allowed us to identify and exploit multiple PFAS···MOF interactions, including coordinative bonding and hydrophobicity, toward enhanced performance. Notably, TFA-MOF-808 exhibits top-performing capture capacities compared to all hitherto reported porous materials for representative short- and long-chain PFAS of global interest. Overall, these results provide new directions on the design of next-generation PFAS sorbents, introducing an effective tailoring strategy while offering unique mechanistic insight. Additional efforts are required to identify the full scope of this research in terms of optimal MOF functionalization and tested contaminants, and we are currently exploring these aspects.

Supporting Information

Supporting Information is available from the Wiley Online Library or from the author.

Acknowledgements

This project has received funding from the European Union's Horizon 2020 research and innovation programme under grant agreement N°101034324. This work was supported by the grants PID2021-123839OB-I00, RYC2018-024328-I, CNS2022-135261, and CNS2023-143965 funded by MICIU/AEI/10.13039/501100011033 and the NextGenerationEU/PRTR. The authors acknowledge the financial support from the Spanish Ministry of Science and Innovation, through the "María de Maeztu" Programme for Units of Excellence in R&D (CEX2018-000805-M). The authors acknowledge the computing facilities of CSUC for providing resources that contributed to the research results reported within this paper. This work was carried out with the support of Diamond Light Source, instrument I15-1 (proposal CY34409-1) and the authors thank Dr Philip Chater for his assistance on PDF experiments. The authors acknowledge the European Synchrotron Radiation Facility (ESRF) for provision of synchrotron radiation facilities (PDF experiments, proposal MA-5852), and the authors would like to thank Stefano Checcia for assistance and support in using beamline ID15A. The authors acknowledge DESY (Hamburg, Germany), a member of the Helmholtz Association HGF, for the provision of experimental facilities. Parts of this research were carried out at PETRAIII and the authors would like to thank Dr. Alba San Jose Mendez for assistance in using beamline P02.1. Beamtime was allocated for proposal I-20230444 EC.

Conflict of Interest

The authors declare no conflict of interest.

Data Availability Statement

The data that support the findings of this study are available in the supplementary material of this article.

Keywords

computational modelling, metal-organic frameworks, per-/polyfluoroalkyl substances, post-synthetic functionalization, water decontamination

Received: June 7, 2024
Revised: July 17, 2024
Published online:

[1] a) S. Kurwadkar, J. Dane, S. R. Kanel, M. N. Nadagouda, R. W. Cawdrey, B. Ambade, G. C. Struckhoff, R. Wilkin, *Sci. Total Environ.* **2022**, 809; b) S. Y. Wee, A. Z. Aris, *npj Clean Water* **2023**, *6*, 57.

[2] a) Fact Sheet: EPA's Proposal to Limit PFAS in Drinking Water; United States Environmental Protection Agency, Washington, D.C, **2023**; b) Commission Delegated Regulation, (EU) 2020/784, OJ L 188I, 15.6.2020, pp. 1–3; c) Directive (EU) 2020/2184, OJL 435, 23.12.2020, pp. 1–62.

[3] a) R. C. Buck, J. Franklin, U. Berger, J. M. Conder, I. T. Cousins, P. D. Voogt, A. A. Jensen, K. Kannan, S. A. Mabury, S. P. J. van Leeuwen, *Integr. Environ. Assess. Manage.* **2011**, *7*, 513; b) C. F. Kwiatkowski, D. Q. Andrews, L. S. Birnbaum, T. A. Bruton, J. C. Dewitt, D. R. U. Knappe, M. V. Maffini, M. F. Miller, K. E. Pelch, A. Reade, A. Soehl, X. Trier, M. Venier, C. C. Wagner, Z. Wang, A. Blum, *Environ. Scie. Technol. Lett.* **2020**, *7*, 532.

[4] R. C. Buck, P. M. Murphy, M. Pabon, in *Polyfluorinated Chemicals and Transformation Products* (Eds.: T. P. Knepper, F. T. Lange), Springer Berlin Heidelberg, Berlin, Heidelberg, **2012**, pp. 1–24.

[5] B. Trang, Y. Li, X. S. Xue, M. Ateia, K. N. Houk, W. R. Dichtel, *Science* **2022**, *377*, 839.

[6] a) S. E. Fenton, A. Ducatman, A. Boobis, J. C. DeWitt, C. Lau, C. Ng, J. S. Smith, S. M. Roberts, *Environ. Toxicol. Chem.* **2021**, *40*, 606; b) E. M. Sunderland, X. C. Hu, C. Dassuncao, A. K. Tokranov, C. C. Wagner, J. G. Allen, *J. Exposure Sci. Environ. Epidemiol.* **2019**, *29*, 131.

[7] a) Z. Du, S. Deng, Y. Chen, B. Wang, J. Huang, Y. Wang, G. Yu, *J. Hazard. Mater.* **2015**, *286*, 136; b) I. Ross, J. McDonough, J. Miles, P. Storch, P. Thelakkat Kochunarayanan, E. Kalve, J. Hurst, S. S. Dasgupta, J. Burdick, *Rem. J.* **2018**, *28*, 101.

[8] a) X. Lei, Q. Lian, X. Zhang, T. K. Karsili, W. Holmes, Y. Chen, M. E. Zappi, D. D. Gang, *Environ. Pollut.* **2023**, *321*, 121138; b) R. Li, N. N. Adarsh, H. Lu, M. Wriedt, *Matter* **2022**, *5*, 3161; c) A. Maimaiti, S. Deng, P. Meng, W. Wang, B. Wang, J. Huang, Y. Wang, G. Yu, *Chem. Eng. J.* **2018**, *348*, 494; d) C. T. Vu, T. Wu, *Environ. Sci.: Water Res. Technol.* **2020**, *6*, 2958.

[9] H. Furukawa, K. E. Cordova, M. O'Keeffe, O. M. Yaghi, *Science* **2013**, *341*, 6149.

[10] a) M. Mon, R. Bruno, J. Ferrando-Soria, D. Armentano, E. Pardo, *J. Mater. Chem. A* **2018**, *6*, 4912; b) S. Naghdi, M. M. Shahrestani, M. Zendehbad, H. Djahaniani, H. Kazemian, D. Eder, *J. Hazard. Mater.* **2023**, *442*, 130127.

[11] L. I. FitzGerald, J. F. Olorunyomi, R. Singh, C. M. Doherty, *ChemSusChem* **2022**, *15*, 202201136.

[12] V. Bon, I. Senkovska, I. A. Baburin, S. Kaskel, *Cryst. Growth Des.* **2013**, *13*, 1231.

[13] H. Furukawa, F. Gándara, Y. B. Zhang, J. Jiang, W. L. Queen, M. R. Hudson, O. M. Yaghi, *J. Am. Chem. Soc.* **2014**, *136*, 4369.

[14] a) V. Bon, I. Senkovska, J. D. Evans, M. Wöllner, M. Hölzel, S. Kaskel, *J. Mater. Chem. A* **2019**, *7*, 12681; b) L. González, R. Gil-San-Millán, J. A. R. Navarro, C. R. Maldonado, E. Barea, F. J. Carmona, *J. Mater. Chem. A* **2022**, *10*, 19606.

[15] I. del Castillo-Velilla, A. Sousaraei, I. Romero-Muñiz, C. Castillo-Blas, A. S. J. Méndez, F. E. Oropeza, V. A. de la Peña O'Shea, J. Cabanillas-González, A. Mavrandonakis, A. E. Platero-Prats, *Nat. Commun.* **2023**, *14*, 2506.

[16] F. Drache, V. Bon, I. Senkovska, C. Marschelke, A. Synytska, S. Kaskel, *Inorg. Chem.* **2016**, *55*, 7206.

[17] a) I. Romero-Muñiz, C. Romero-Muñiz, I. Del Castillo-Velilla, C. Marini, S. Calero, F. Zamora, A. E. Platero-Prats, *ACS Appl. Mater. Interfaces* **2022**, *14*, 27040; b) R. Thür, N. Van Velthoven, V. Lemmens, M. Bastin, S. Smolders, D. De Vos, I. F. J. Vankelecom, *ACS Appl. Mater. Interfaces* **2019**, *11*, 44792.

[18] a) D. Camdzic, R. A. Dickman, D. S. Aga, *J. Hazardous Mater. Lett.* **2021**, *2*, 100023; b) D. A. Ellis, K. A. Denkenberger, T. E. Burrow, S. A. Mabury, *J. Phys. Chem. A* **2004**, *108*, 10099; c) T. M. Vanoursouw, T. Rottiger, K. A. Wadzinski, B. E. Vanderwaal, M. J. Snyder, R. T. Bittner, O. K. Farha, S. C. Riha, J. E. Mondloch, *J. Chem. Educ.* **2023**, *100*, 861.

[19] M. F. Rahman, S. Peldszus, W. B. Anderson, *Water Res.* **2014**, *50*, 318.

[20] a) F. Li, J. Duan, S. Tian, H. Ji, Y. Zhu, Z. Wei, D. Zhao, *Chem. Eng. J.* **2020**, *380*, 122506; b) M. Scheurer, K. Nödler, F. Freeling, J. Janda, O. Happel, M. Riegel, U. Müller, F. R. Storck, M. Fleig, F. T. Lange, A. Brunsch, H. J. Brauch, *Water Res.* **2017**, *126*, 460; c) G. Zheng, S. M. Eick, A. Salamova, *Environ. Sci. Technol.* **2023**, *57*, 15782.

[21] M. Sun, J. Cui, J. Guo, Z. Zhai, P. Zuo, J. Zhang, *Chemosphere* **2020**, *254*, 126894.

[22] a) R. Li, S. Alomari, R. Stanton, M. C. Wasson, T. Islamoglu, O. K. Farha, T. M. Holsen, S. M. Thagard, D. J. Trivedi, M. Wriedt, *Chem. Mater.* **2021**, *33*, 3276; b) R. R. Liang, S. Xu, Z. Han, Y. Yang, K. Y. Wang, Z. Huang, J. Rushlow, P. Cai, P. Samorì, H. C. Zhou, *J. Am. Chem. Soc.* **2024**, *146*, 9811.

[23] Y. Zhi, J. Liu, *Environ. Pollut.* **2015**, *202*, 168.

[24] a) I. del Castillo-Velilla, I. Romero-Muñiz, C. Marini, C. Montoro, A. E. Platero-Prats, *Nanoscale* **2024**, *16*, 6627; b) A. E. Platero-Prats, A. Mavrandonakis, L. C. Gallington, Y. Liu, J. T. Hupp, O. K. Farha, C. J. Cramer, K. W. Chapman, *J. Am. Chem. Soc.* **2016**, *138*, 4178; c) H. Xu, S. Sommer, N. L. N. Broge, J. Gao, B. B. Iversen, *Chem.–Eur. J.* **2019**, *25*, 2051.

[25] H. Omorodion, B. Twamley, J. A. Platts, R. J. Baker, *Cryst. Growth Des.* **2015**, *15*, 2835.

[26] H. Omorodion, M. Palenzuela, M. Ruether, B. Twamley, J. A. Platts, R. J. Baker, *New J. Chem.* **2018**, *42*, 7956.

[27] G. V. Janjić, S. T. Jelić, N. P. Trišović, D. M. Popović, I. S. Dordević, M. K. Milčić, *Cryst. Growth Des.* **2020**, *20*, 2943.